Nanoscale

Accepted Manuscript

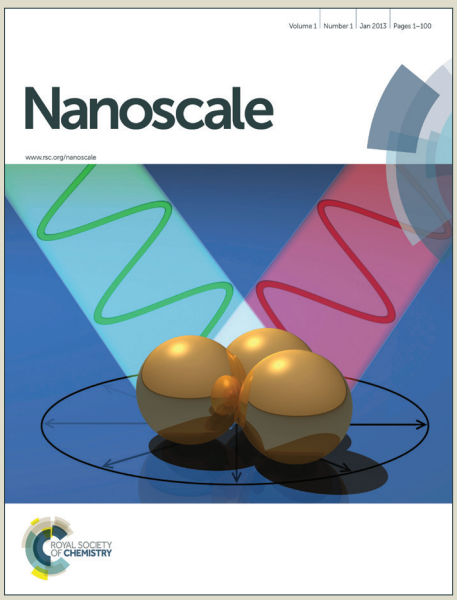

ROYAL SOCIETY OF CHEMISTRY

www.rsc.org/nanoscale

Cite this: DOI: 10.1039/c0xx00000x

www.rsc.org/xxxxxx

ARTICLE TYPE

Iron Oxides Nanoparticles Immobilized to Mesoporous NH_2-SiO_2 Spheres by Sulfonic Acid Functionalization as Highly Efficient Catalysts

Guoliang Zhang,[a] Lei Qin, [a] Yujiao Wu, [a] Zehai Xu [a] and Xinwen Guo [b]*

Received (in XXX, XXX) Xth XXXXXXXXX 20XX, Accepted Xth XXXXXXXXX 20XX

DOI: 10.1039/b000000x

A novel SiO_2 nanosphere was synthesized by post-synthetic grafting of sulfonic acid groups on anionic-surfactant-templated mesoporous NH_2-silica (AMAS). The one-pot post-functionalization strategy allowed more metal ions to be homogeneously anchored into the channel of meso-SiO_2 nanosphere. After hydrothermal and calcination treatment, in situ growth of α-Fe_2O_3 on sulfonic acid-functionalized mesoporous NH_2-SiO_2 (SA-AMAS) exhibited much higher activity in visible-light assisted Fenton reaction at neutral pH than that for AMAS or meso-SiO_2 nanosphere. By analysis, the grafted sulfonic acid group can not only enhance the acid strength of catalyst, but also bring more orbital-overlapping between active sites ($Fe^{□}$ and $Fe^{□}$) and surface peroxide species to facilitate the decomposition of H_2O_2 to hydroxyl radical. The present results will make opportunities for developing of heterogeneous catalysts with high-performance in the field of green chemistry and environmental remediation.

1. Introduction

Mesoporous silica, as a kind of highly ordered porous materials, has enormous potentiality in field of molecules adsorption, separation, chemical sensing, and catalysis.[1-4] In recent years, more attention has been focused on immobilizing of metal or metal oxides to mesoporous silica for heterogeneous catalytic reaction (such as Fenton oxidation) due to the uniform and adjustable pore size, well-defined channel and large surface area.[5-9] However, the introduction of nanoclusters on the surface of solid has often caused the reduction of activity due to detrimental interaction with support or mutual deactivation between too close sites, which limits the wide application of supported catalyst.[10] To overcome these drawbacks, some efforts have been devoted to incorporate iron oxide nanoparticles (NPs) inside alumina-coated mesoporous silica (MCM-41 and SBA-15) for increasing the dispersion of NPs.[11] But the thickness and the location of alumina-coating is often hard to control, and consequently influence the activity of catalysts. Therefore, developing a rational method to immobilize single active sites within the support is essential.

Surface functionalization may guide us towards a highly promising alternative for improving dispersion of active sites on the surface of supports and enhancing the binding force between them. It is noteworthy that many organic groups such as -NH_2, -COOH and -SH can be bonded with silanol groups (Si-OH) on the pore wall of mesoporous silica, and then obviously change its surface properties.[12-15] Among various functionalized groups, sulfonic acid introduced has significant effect on catalytic activity of the catalysts due to strong interaction with metal sites and surface acid property.[16] In most previous studies, sulfonic acid-functionalized mesoporous SiO_2 was prepared by co-condensation and subsequent oxidation method.[17] However, only a few disordered sulfonic acid groups were exposed on the surface of pores, which may contribute to the aggregation of nanoparticles on out surface of host matrix and the decrease of catalytic activity.[18,19] A general and facile method for controllable preparation of sulfonic acid groups well-dispersed on the surface of mesopores is still a big challenge.

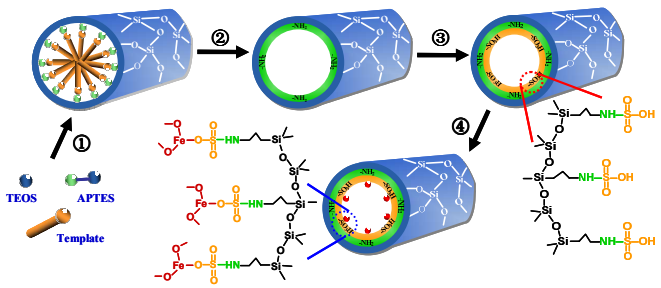

Scheme 1 Synthesis procedure of sphere structured Fe_2O_3/sulfonic acid-functionalized mesoporous NH_2-SiO_2 nano material. Steps 1–4 refer to the hydrothermal reaction, ion-exchange extraction, post-synthetic grafting with chlorosulfuric acid in CH_2Cl_2 solution, and loading by impregnating-hydrothermal method and subsequent calcination, respectively.

The postsynthetic modification is considered as a powerful tool for obtaining highly sophisticated functionalized structures, which means the introduction of functionalities after framework synthesis.[20] In this study, we propose a new strategy of one-pot post-synthetic grafting of sulfonic acid groups on mesoporous SiO_2 nanosphere which depends on the strong electrostatic interaction with the surface amino groups (Scheme 1). In

comparison with in situ co-condensation, the method not only simplifies the fabrication technology and improves the controllability, but also offers a good opportunity for sulfonic acid groups to highly disperse on the surface of mesopores. Different from conventional surface grafting methods, the key factor to success is making use of the amino-functionalized mesoporous silica nanospheres synthesized by an anionic surfactant templating route.[21-24] The amino-organic moieties in the one-pot post-synthetic process can homogeneously distribute near the opening of channel and/or on external surface of the silica wall with a high loading.

Based on this new idea, iron oxide nanoparticles immobilized on the mesoporous NH_2-SiO_2 nanospheres by sulfonic acid functionalization were fabricated for the first time. The possibility to make use of Fe_2O_3 supported nanosphere for facilitating the heterogeneous photo-Fenton process was investigated in detail. By characterizing the structure and measuring the properties of SiO_2-based catalyst, the structure-activity relationship in hybrid materials was analyzed. The synergetic effect of nanoparticles and functional groups of support on the catalytic reaction was evaluated.

2. Experimental section

2.1 Chemicals

The commercial azo dye Reactive Brilliant Red X-3B was available from Betapharma (Shanghai, China) and used without further purification. (3-aminopropyl) triethoxy-silane (APTES), N-Lauroylsarcosine sodium salt (Sar-Na), Tetraethyl orthosilicate (TEOS), ethanol amine, chlorosulfonic acid ($ClSO_3H$, 98% wt.%), $Fe(NO_3)_3{\cdot}9H_2O$, HCl (35 wt.%), anhydrous ethanol, dry CH_2Cl_2, H_2O_2 (30%, wt.%) were of analytical grade and purchased from Sinopharm Chemical Reagent Co., Ltd. The deionized water used in experimental solutions was manufactured by a self-made RO-EDI system, in which ion concentration was analyzed by IRIS Intrepid ICP and Metrohm 861 Compact IC and controlled to meet the requirement of conductivity $\sigma \leq 0.5$ μS cm^{-1}.

2.2 Materials synthesis

Anionic surfactant-templated mesoporous silicas were synthesized according to the method described by Wang et al.[25] Typically, 0.5868 g (2 mmol) Sar-Na was dissolved in 70 ml deionized water at room temperature by continuous stirring. Then, 13 g of HCl solution (0.1 M) was added to the above solution and kept strong agitation. Subsequently, a mixture of 0.25 ml APTES and 3.0 ml TEOS was added to the prepared solution. After stirring, the resulting emulsion was aged for a while at room temperature, and then transformed into a 200 ml Teflon-lined autoclave container and held at 353 K for 24 h. Finally, the product was washed with distilled water and dried under vacuum condition. Removing the surfactant from obtained solids was obtained by two methods including ion-exchange extraction and calcination.[26] In ion-exchange extraction process, the as-prepared sample was dispersed in mixture solution of ethanol and ethanol amine, which was stirred and refluxed at 363 K for 12 h. The obtained product was washed with ethanol and dried under vacuum condition. In the calcination process, the as-prepared sample was calcined at 823 K for 4 h. The calcination of as-synthesized samples leads to the removal of both the surfactant and organic moieties derived from the co-structure-directing agent (CSDA), resulting in the generation of purely inorganic silica (AMS), but the aminopropyl groups also existed in mesoporous silica by using ion-exchange extraction method. The obtained amino-functionalized AMS was remarked as AMAS.

The sulfonic acid-functionalized AMAS was prepared by post-synthetic grafting method.[27] Typically, 1.0 g AMAS was dispersed in CH_2Cl_2 (15 mL) under ultrasonic bath. Then, 4 mL chlorosulfuric acid was added dropwise over a period of 30 min under ultrasonic condition. After standing, the supernatant was discarded and as-prepared functionalized AMAS nanoparticles were washed with CH_2Cl_2 in order to remove the unattached substrates on the surface of solids. The obtained products were dried under vacuum and abbreviated as SA-AMAS.

Fe_2O_3 was immobilized into mesoporous silica nanospheres by impregnating-hydrothermal method and subsequent calcination. Modified silica nanospheres (AMS, AMAS, and SA-AMAS) were dispersed in 100 ml deionized water, and then a certain amount of $Fe(NO_3)_3{\cdot}9H_2O$ (metal ion/silica = 8%, w/w) was added to the above suspension. After stirring, the impregnating solution was transformed into a 200 ml Teflon-lined autoclave kettle and held at 353 K for 12 h. The product was washed with deionized water, and dried in a vacuum oven. Finally, the as-synthesized powders were calcined at 523 K for 6 h. The resulting deep yellow samples were labelled as Fe_2O_3/AMS, Fe_2O_3/AMAS, and Fe_2O_3/SA-AMAS, respectively.

2.3 Characterization

Surface morphology was observed by scanning electron microscopy (SEM, Hitachi TM-1000) and transmission electron microscopy (TEM, Hitachi EM-1200EX) images. The composition analysis of the samples were analyzed by energy-dispersive X-ray spectra (EDS) attached together with micrograph using field emission scanning electron microscopy (FESEM, F.E.I XL30-ESEM TMP) at an accelerating voltage of 15.0 kV. N_2 adsorption-desorption isotherms at 77 K were derived from an ASAP2010 (Micromeritics, USA) analyzer, and the surface area, pore volume, as well as pore size distribution were calculated by conventional BET and BJH methods. Prior to the measurement, the samples were degassed at 473 K. XRD spectra of the powdered samples were recorded using an X'Pert PRO X-ray diffractometer equipped with a Cu Kα radiation (λ=1.5418Å, 40 kV, 40 mA). Data were collected from 2θ = 10°-80° with a 0.02° step size. FT-IR spectroscopy was conducted to study the surface functional groups, which were obtained on a Nicolet 6700 Fourier transform infrared spectrometer (Thermo, USA) operated in transmission mode (400-4000 cm^{-1}) at a resolution of 4.0 cm^{-1} with the sample as KBr pellets. XPS measurements were performed on a RBD upgraded PHI-5000C ESCA system (Perkin-Elmer) with Mg Kα X-ray source (hv=1253.6 eV). To correct for charging effects, all spectra were calibrated relative to a carbon 1s peak positioned at 284.6 eV. The acid properties of the catalysts were characterized using FTIR spectroscopy of pyridine adsorption (Py-IR), which were recorded on an EQUINOX55 Fourier transform infrared spectrometer (Bruker, German) at 4 cm^{-1} resolutions.

2.4 Catalytic experiments

Reactive Brilliant Red (X-3B), a kind of azo dye, was chosen as aqueous model pollutant. The oxidation of 100 mg·L^{-1} X-3B with H_2O_2 at visible light irradiation (200 W halogen lamp, emission wavelength: 350-450 nm) was carried out with a total volume of 100 ml, using a certain quantity of catalyst. All glass reactors were kept oscillation at 298 K in a thermostatic water bath oscillator. The initial pH value of dye solutions were adjusted by using HCl and NaOH solutions (0.1 M) to the required value, and the lamp was hung over the reactors. Before reaction, the suspension was stirred continuously in darkness for 30 min to ensure the equilibrium adsorption.

The concentration of dye in samples was measured by U-2910 digital spectrophotometer (Hitachi, Japan) after filtered directly through 0.45 μm microfiltration membrane. Samples for total organic carbon (TOC) analysis were immediately treated with 0.15 M Na_2SO_3 scavenging reagent and centrifuged to separate catalyst, then determined by using a TOC analyzer (TOC-V cph, Shimadzu). Iron content of the reaction solution was measured by a flame atomic absorption spectrometry (Spectr-AA-55B, Varian) equipped with hollow cathode Fe lamp (sensitive line: 248.3 nm; slits: 0.4 nm; operating current: 4 mA). The variation of H_2O_2 decomposition rate was analyzed by colorimetric method using UV-vis spectrophotometer after complexation reaction with titanium salt.[28]

3. Results and discussion

3.1 Catalysts characterization

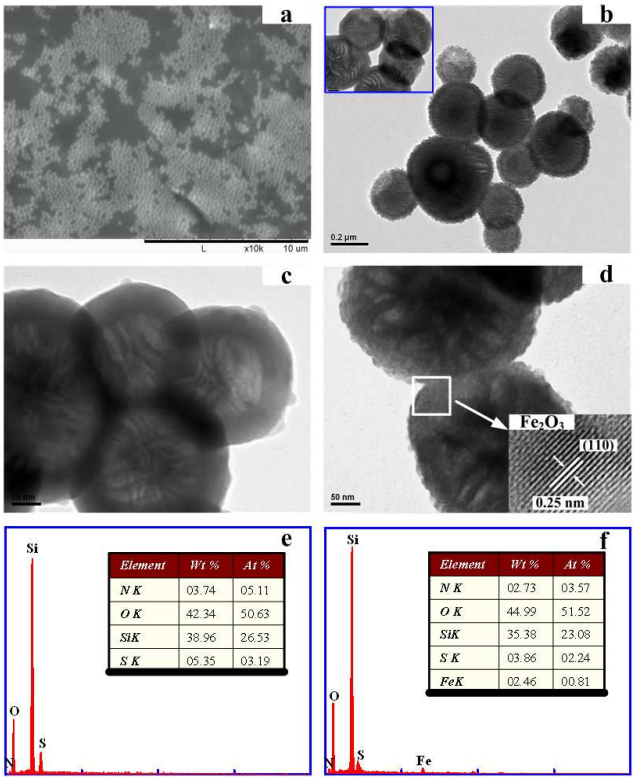

Fig. 1 SEM image of monodispersed AMAS (a) and TEM images of AMAS (b), SA-AMAS (c), and Fe_2O_3/SA-AMAS (d); and EDX spectrum of SA-AMAS (e) and Fe_2O_3/SA-AMAS (f). The inset is HRTEM image of lattices of Fe_2O_3.

Surface morphology and chemical composition of the samples in different phases were characterized by means of SEM, TEM and EDS. The typical SEM and TEM images of AMAS are shown in Fig. 1(a, b). It presents a good spherical-like structure and highly oriented growth behavior after ion-exchange extraction process. AMAS has a typical diameter of 100-200nm, and a highly mesoporous texture clearly appears as white objects inside sphere due to the removing of surfactant. As illustrated by TEM images (Fig. 1b and c), it is found that the morphology of the nanosphere does not change after postfunctionalization, but the pores of SA-AMAS are narrower than AMAS, indicating that sulfonic acid functional groups have successfully entered into the channels of AMAS. Meanwhile, EDX pattern of SA-AMAS (Fig. 1e) also reveals the presence of the S element inside the pore channel. After decorated with Fe_2O_3, it is clear that the morphology and mesoporous network of the SA-AMAS host remain intact (Fig. 1d). Importantly, TEM image gives an obvious evidence for iron oxide nanoclusters which are uniformly dispersed in the cavities of support matrix not aggregated on the surface. The lattice fringe spacing of the supported nanoparticle was 0.25 nm corresponding to the (110) crystallographic plane of the α-Fe_2O_3 crystal (see the inset of Fig. 1d).[29] Fig. 1f shows the EDX pattern of the supported nanosphere, which confirms iron oxide and sulfur species existing on the channel of SA-AMAS host (Fig. 1f) after hydrothermal and sintering process.

The Nitrogen adsorption/desorption isotherms and pore size distribution curve were investigated to evaluate the surface area and pore size distribution of the prepared nanospheres. Seen from Fig. 2, the isotherms of all the catalysts show a typical IV type pattern with a hysteresis loop in the low relative (P/P_0) range, which well validate the occurrence of mesopores. The distribution of pore diameter is mainly located between 2.0 and 10.0 nm. As apparent from Table S1, an increase in BET surface area is observed for AMAS after sulfonic acid-functionalization, which is in favor of the surface adsorption and mass transfer. In comparison with SA-AMS, the loading is accompanied by an appreciable decrease in BET, pore size and pore volume of sample Fe_2O_3/SA-AMAS, indicating that in situ growth of nanoclusters occupy the pores of SiO_2 nanosphere during heat treatment.

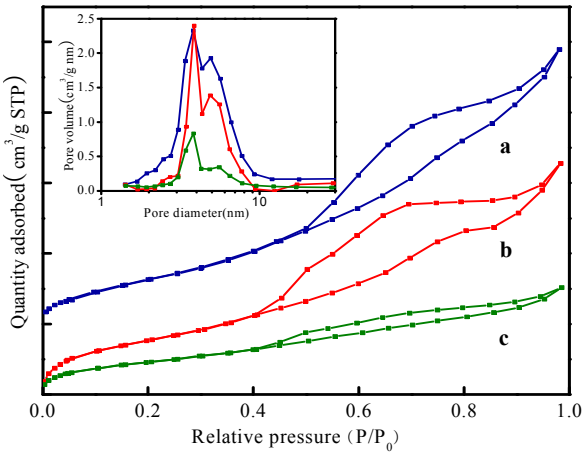

Fig. 2 Nitrogen adsorption/desorption isotherms and BJH pore size distribution of (a) AMAS, (b) SA-AMAS and (c) Fe_2O_3/SA-AMAS.

Fig. 3(A) records the FTIR spectrum of AMAS, SA-AMAS, and Fe_2O_3/SA-AMAS. The asymmetric and symmetric stretching vibration peaks at 1088 and 812 cm^{-1} are assigned to the host framework of Si-O-Si, as well as the intense bending vibration

band at 463 cm^{-1}.[30] In comparison with AMAS, the stronger absorption peak at 3400 and 1627 cm^{-1} is observed for sample SA-AMAS, which indicates that more dissociative hydroxyl groups and molecular H_2O are adsorbed on the sulfonic acid-functionalized nanospheres due to strong hydrophilicity of -SO_3H group. According to the previous studies, the absorption peaks around 2852 and 2932 cm^{-1} correspond to the stretching vibration of the methylene groups for surfactant and CSDA, respectively.[31] It is worth to note that stretching band at 2932 cm^{-1} remains, but the peak around 2852 cm^{-1} disappears, demonstrating that the surfactant has been removed by ion-exchange extraction method without destruction of CSDA. Moreover, the -NH group of CSDA is reflected from bending vibration peak at 687 cm^{-1}.[32] Compared with AMAS, a decrease in the intensity of -NH characteristic peak is observed for SA-AMAS, which may be attributed to the generation of -NH-SO_3H group. In the curve of SA-AMAS, it is evident that the sulfur species appear accompanying by characteristic peaks at 1495 cm^{-1}, and a new absorption peak at 608 cm^{-1} is attributed to the bending vibration of hydrogen bond between the OH and SO_3H groups.[33-35] However, these characteristic peaks intensities decrease dramatically after supporting with iron oxide, which clearly suggests that sulfonic acid group of AS-AMS carrier has been shielded due to chemical bond with Fe_2O_3 nanoparticles.[36]

Due to O=S=O groups acting as the electron withdrawing species, more strong acid sites (Brønsted and Lewis) occur inside of nanosphere tunnel (Fig. 3B), which can not only improve the adsorption of substance, but also reduce the pH value of surrounding and accelerate the decomposition of H_2O_2 to generate hydroxyl radicals.

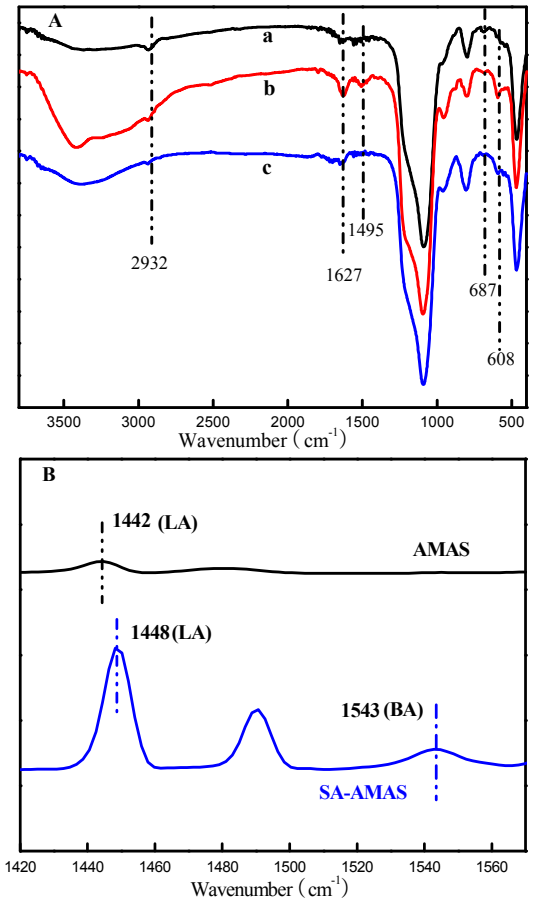

Fig. 3 (A) FTIR spectra of (a) AMAS, (b) SA-AMAS and (c) Fe_2O_3/SA-AMAS. (B) Py-IR spectra of the AMAS and SA-AMAS.

The crystalline structures of different samples are presented in Fig. 4. In the diffraction patterns, the broad characteristic peak at approximately 2θ=23° corresponds to the amorphous silica. When SA-AMAS are loaded by iron oxide, other four weak diffraction peaks at 2θ= 33.21, 40.70, 53.85 and 63.72° are clearly observed, which are the reflections from the (104), (113), (116) and (300) planes of hematite (α-Fe_2O_3) crystallite, respectively. This reveals that small and well-dispersed α-Fe_2O_3 nanoparticles are formed inside the pores of SA-AMS due to the sulfonic group retarding crystallite agglomeration, consistent with TEM image.[37]

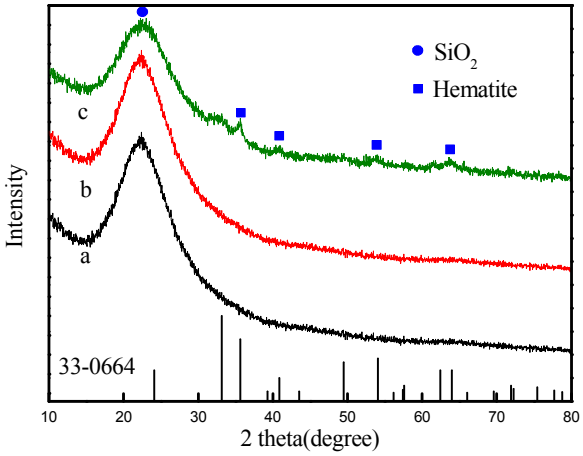

Fig.4 X-ray diffraction patterns of (a) AMAS, (b) SA-AMAS and (c) Fe_2O_3/SA-AMAS.

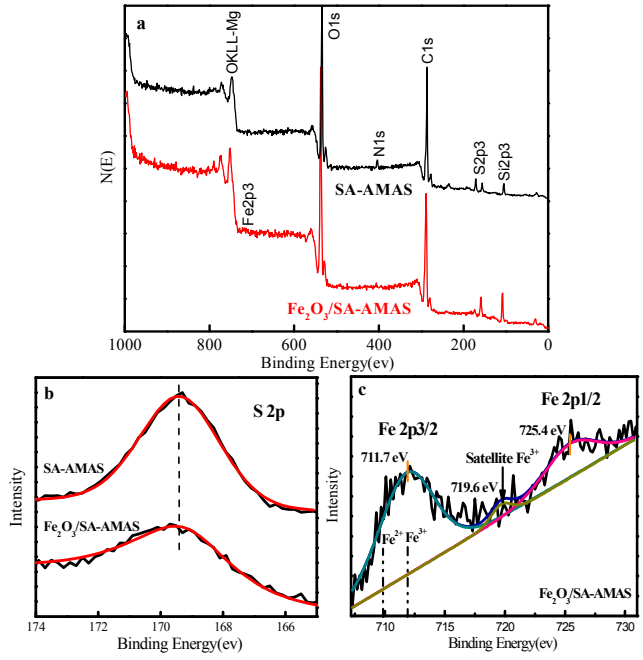

Fig.5 XPS spectra of different samples: (a) full spectra of SA-AMAS and Fe_2O_3/SA-AMAS and fine XPS spectra of (b) S 2p, (c) Fe 2p.

To investigate the chemical state of iron oxides supported on SA-AMAS, XPS measurement was carried out and the results are presented in Fig. 5. In the XPS spectra curve of SA-AMAS and Fe_2O_3/SA-AMAS, the presence of O1s, Si2p, N1s, S2p, and Fe2p can be ascertained (Fig. 5a). As depicted in in Fig. 5b, the binding energy of S2p peak for sample SA-AMS is observed at 169.4 eV, which is assigned to the spectra of -NH-SO_3H.[38] After Fe_2O_3

loading, a slight shift (0.2 eV) to lower energy of S2p peak can be observed compared to bare SA-AMAS, indicating the increasing in electron density of S2p. This shift can be ascribed to the formation of -SO_3-Fe-O bond in the composites, which is in agreement with the FTIR results. In the fitting curve of the sample Fe_2O_3/SA-AMAS (Fig. 5c), the binding energy of the Fe 2p is observed at 711.7 and 725.4 eV, which is assigned to the spectra of Fe 2p1/2 and Fe 2p3/2 for the lattice Fe^{III}-O in Fe_2O_3, respectively.[29b] The contribution at around 709.8 eV belongs to the Fe^{II}-O, while the contribution of binding energy at 719.6 eV is assigned to the surface iron species and satellite signal of the Fe^{3+} species.

3.2 Catalytic activity

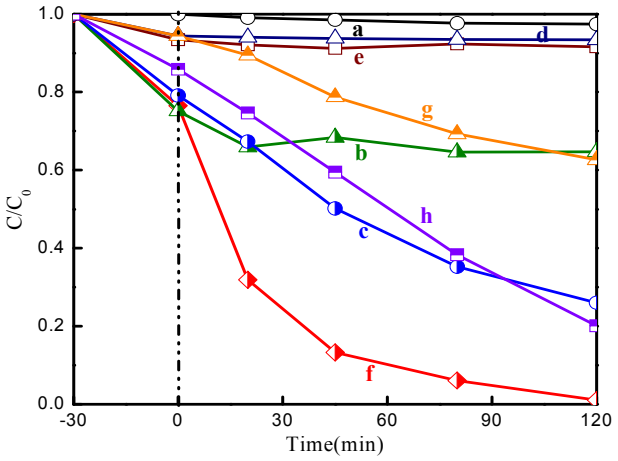

Fig. 6 Relative concentration of X-3B as a function of time at different procedures: (a) Vis+H_2O_2 (b) Vis+Fe_2O_3/SA-AMAS (c) Fe_2O_3/SA-AMAS+H_2O_2 (d) Vis+Fe_2O_3/AMS+H_2O_2 (e) Vis+Fe_2O_3/AMAS+H_2O_2 (f) Vis+Fe_2O_3/SA-AMAS+H_2O_2 (T=298 K, pH=6.0, C_{cat}=0.5 g·l^{-1}, $C_{X\text{-}3B,\,0}$=100 m g·l^{-1}, $C_{H2O2,\,0}$=5.0 mM), (g) Vis+0.5 g·$l^{-1}$$Fe_2O_3$/ AMS+5.0 mM H_2O_2 (pH=4.0), (h) Vis+0.5 g·l^{-1} Fe_2O_3/AMAS+5.0 mM H_2O_2 (pH=4.0).

The Fenton-like degradation of toxic and recalcitrant organic pollutants is of great importance in environmental protection and provides a commonly used way to test the activities of prepared catalysts. Fig. 6 shows the efficiency of different catalytic oxidation for the degradation of dye X-3B. Under visible irradiation, X-3B was stable only with Fe_2O_3/SA-AMAS in absence of H_2O_2, which indicated that the photocatalytic reaction did not proceed and decolorization was due to the adsorption of solid. However, 74.0 % of X-3B was degraded by Fe_2O_3/SA-AMAS/H_2O_2 system in the dark (curve d), which demonstrated that decomposition of hydrogen peroxide to ·OH radical can be catalyzed by ≡Fe^{III} active sites inside SA-AMAS support. Under the cooperative effect of H_2O_2 and light irradiation, Fe_2O_3/SA-AMS exhibited superior catalytic performance for dye degradation at pH of 6.0 (99.0 % photobleaching). It is well verified that light radiation can promote the electron transfer of Fe^{II}/Fe^{III} and subsequently facilitate the ·OH radical production.[39,40] In this study, methanol and 2-propanol have been used as the trapping agents to illustrate the evidence of ·OH radicals in the catalytic oxidation process (Fig. S1). It is clear that a rapid decrease in the degradation efficiency of dye was observed from 99.0 to 51.5 and 53.3 % after adding the methanol and 2-propanol, respectively. It well indicates that lots of ·OH radicals was produced in the aqueous solution and played an important role on the oxidation of dyes. The effects of pH, catalyst loading and H_2O_2 dosage on catalytic activity of Fe_2O_3/SA-AMAS are presented in the supporting information (Fig. S2-4).

In order to better understand the effect of incorporation of sulfonic acid groups on performance of the catalysts, we also prepare Fe_2O_3/AMS and Fe_2O_3/AMAS and investigate their photocatalytic ability in this study. Result shows that both Fe_2O_3/AMS and Fe_2O_3/AMAS underwent slight degradation of dye at initial pH of 6.0. While the initial pH of solution decreased to 4.0, 37.3 and 80.0 % of degradation efficiency were observed for Fe_2O_3/AMS and Fe_2O_3/AMAS, respectively. This reveals that the grafting of functional groups on mesoporous SiO_2 nanosphere could enhance the activity of supported catalysts. However, in comparison with amino group, introduction of sulfonic acid group can greatly widen the working pH range and improve the surface adsorption of substances.

The loading method and calcination temperature on the catalytic activity of Fe_2O_3/SA-AMAS is highlighted in Fig. 7. In sharp contrast, impregnating-hydrothermal-calcination made the composite materials exhibit higher activity in Fenton-like reactions than the other two treatments. It implies that the generation of highly active sites inside the pore of support should be experienced multi-treatment. Moreover, calcination temperature also determined the catalytic activity. As apparent from figure, the highest activity of Fe_2O_3/SA-AMAS was observed at 523 K. As the temperature exceeding 523 K, an obvious decrease in the degradation efficiency of X-3B was obtained with the increase of temperature, and the activity of solid could be lost at 773K. According to report by Hao et al, the most organic groups of CSDA were combusted during calcination process in the temperature range of 673-883 K. Therefore, it was considered that the activity of active sites was closely associated with the characteristics of functional groups on support.[41]

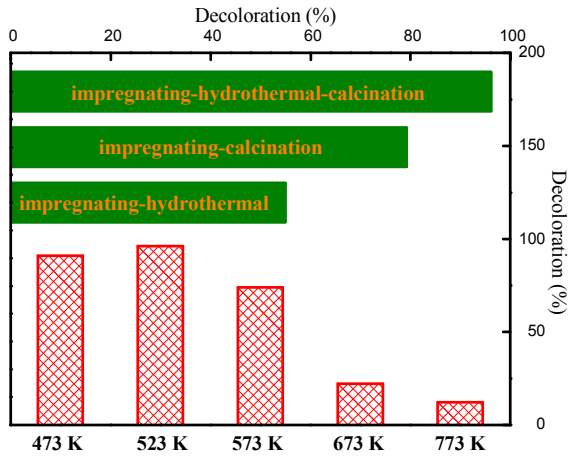

Fig. 7 Effect of loading method and calcination temperature on the dye degradtion by using SA-AMAS as support.

The influence of the Fe loading amount on the catalytic activity is presented in Fig. S5. A remarkable increase in the degradation efficiency of X-3B is observed from 86.3 to 99.0 % with Fe content increasing from 6.0 to 8.0 wt%. This is due to more active sites for the decomposition of hydrogen peroxide to ·OH radicals. However, when the Fe content was further increased to 15.0 wt%, the lower photobleaching efficiency of X-3B (91.6 %) was obtained. In addition, the concentration of

leached Fe ion obviously increased in the Fe content range of 10.0 to 15.0 wt%, which demonstrated that a number of iron oxides could not be stabilized inside the pore of mesoporous sphere. These results appear to indicate that the iron oxides bonding with the -SO_3H groups of support play a more important role in the enhancement of catalytic activity.

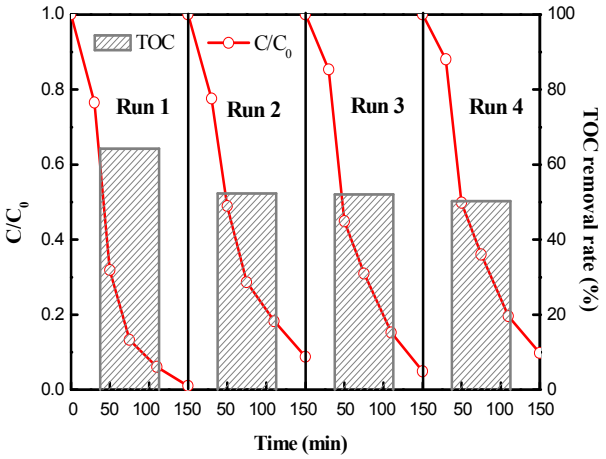

Fig. 8 Reusability of catalysts after subsequent reactions (T=298 K, initial pH=6.0, $C_{Cat.}$= 0.5 g L^{-1}, $C_{X\text{-}3B,\ 0}$=100 mg L^{-1}, $C_{H2O2,\ 0}$=5.0 mM).

3.3 Catalyst stability

The reusability of catalyst is important factor for practical application. Under the optimum conditions, the recycling tests were carried out to evaluate the stability of catalyst reused (Figure 9). After washing with methanol and thermal treatment, the catalysts can be reused for at least four catalytic runs without significant loss of activity as the decoloring and mineralization ratio of dye was as high as 90.2 and 50.3 % for all four runs. Despite a slight decline was found in the second run, by contrast, the catalytic activity had almost no change in the last three runs. The leaching of iron ions during the reaction process remained below 0.24 mg·L^{-1} in all three cycles, which had insignificant influence on the catalytic performance (Fig. S6). FT-IR spectrum also points out that the functional groups were remained on the surface of solid after multiple uses in catalysis (Fig. S7). It was clear that the Fe_2O_3/SA-AMAS nanosphere was stable and resistant to photo-corrosion because a stable bridge of -$NHSO_3$- between the metal ions and the support was developed. This also well demonstrated that sulfonic acid-functionalized mesoporous NH_2-SiO_2 provided a strong stabilization of small metal oxide NPs highly dispersed in the porous matrix.

3.4 Effect of structure and property of support on catalytic activity

As commented, Fe_2O_3/SA-AMAS exhibited much higher catalytic activity than Fe_2O_3/AMS and Fe_2O_3/AMAS in the experiment. The outstanding activity of the catalyst was attributed to the existence of organic groups on SiO_2 nanosphere, which had a significant effect on the control of size and location of metal oxides NPs and the interaction between active sites and support. As shown in Scheme 2, more Fe^{3+} ions existed in solution were inclined to integrate with mesoporous SiO_2 nanosphere (AMS) depending on weak van der Waals forces and stabilize at external surface of support to form large iron oxides NPs. The particle size of aggregates was larger than 20 nm. When amino-functionalized mesoporous SiO_2 nanosphere (AMAS) was used as support, Fe^{3+} ions were coordinated with the amino groups at the mesopore walls, preventing the NPs aggregated on out surface of host matrix. However, lots of the particles agglomerated together inside the cavities of nanosphere, which may be attributed to weak interaction between metal ions and amino groups. Grafting of -SO_3H on AMAS established strong interaction between metal ions and SiO_2 nanosphere through forming strong covalent bond, and provided steric restrictions to confine the growth of metal oxides on surface of pores. It was apparent that more small NPs with average diameter of 2.8 nm uniformly located in mesopores. Sulfonic groups played a location-directing role in incorporating NPs into the cavities of SiO_2. Meanwhile, element analysis of supported materials at three points was presented in supporting information (Fig. S8). It can be concluded that high dispersion of ultrafine activate sites in mesoporous frameworks of SiO_2 nanosphere had a positive effect on the activity of catalysts.

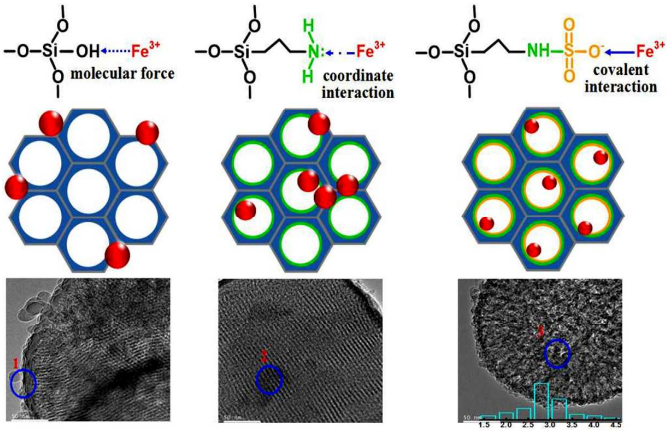

Scheme 2 Schematic diagram of size and location of Fe_2O_3 NPs supported on AMS, AMAS, and SA-AMAS.

Moreover, the grafted sulfonic acid groups played an important role in catalytic oxidation reaction by improving the surface acid property. The generated acid sites can not only have a positive effect on the anchoring of reactant and H_2O_2 molecules to the surface of catalyst due to strong electrostatic pull, but also be in favour of the separation of photo-induced electrons and holes of active sites.[42,43] Besides, the -SO_3H group bonding with Fe^{III} would take up more extended space, which resulted in more orbital-overlapping between the Fe^{III} and surface peroxide species.[44]

4. Conclusions

In summary, we developed a novel one-pot sulfonic acid post-functionalization of anionic-surfactant-templated mesoporous NH_2-silica (AMAS) enabling the immobilization of iron oxides nanoparticles in its pores. Characterization results show that sample SA-AMAS presented high specific surface area, strong hydrophilicity and lots of acid sites. The sulfonic acid functional groups grafted on AMAS can not only lead many α-Fe_2O_3 nanoparticles uniformly disperse in the channels of support, but also make Fe_2O_3/SA-AMS exhibit excellent catalytic activity toward X-3B degradation in visible-light irradiation at neutral

pH. Moreover, the stability of catalyst was significantly improved through the stable bridge between the metal ions and sulfonic group of support. Thus, the progresses presented here are very helpful not only in developing the highly-efficient and green heterogeneous catalysts for environmental remediation, but also in providing a valuable insight for understanding the relationship between the properties of support and catalytic activity.

Acknowledgements

This work was supported by the National Natural Science Foundation of China (No. 21236008 and 21476206).

Notes and references

[a] *Institute of Oceanic and Environmental Chemical Engineering, College of Chemical Engineering and Material Science, Zhejiang University of Technology, Hangzhou 310014, China; Fax/ Tel:86 571 88320863; E-mail: guoliangz@zjut.edu.cn*

[b] *State Key Laboratory of Fine Chemicals, Department of Catalysis Chemistry and Engineering, Dalian University of Technology, Dalian 116012, China*

† Electronic Supplementary Information (ESI) available: BET surface area and textural data, degradation results, FTIR spectra, TEM images, and element analysis. See DOI: 10.1039/b000000x/

1 C. T. Kresge, M. E. Leonowicz, W. J. Roth, J. C. Vartuli and J. S. Beck, *Nature* 1992, **359**, 710-712.

2 J. S. Beck, J. C. Vartuli, W. J. Roth, M. E. Leonowicz, C. T. Kresge, K. D. Schmitt, C. T.-W. Chu, D. H. Olson, E. W. Sheppard, S. B. McCullen, J. B. Higgins and J. L. Schlenkert, *J. Am. Chem. Soc.*1992, **114**, 10834-11843.

3 S. Kim, J. Ida, V. V. Guliants and J. Y. S. Lin, *J. Phy. Chem. B* 2005, **109**, 6287-6293.

4 C. Kind, R. Popescu, E. Müller and C. Feldmann, *Nanoscale*, 2010, **2**, 2223-2229.

5 A. M. El-Toni, M. W. Khan, M. A. Ibrahim, M. Abid, M. Al-Hoshan and M. Al-salhi, *Chem. Comm.* 2010, **46**, 6482-6484.

6 J. M. Zheng, Y. L. Dong, W. F. Wang, Y. H. Ma, J. Hu, X. J. Chen and X. G. Chen, *Nanoscale*, 2013, **5**, 4894-490.

7 B. Lee, Z. Ma, Z. Zhang, C. Park and S. Dai, *Microporous Mesoporous Mater.* 2009, **122**, 160-167.

8 H. S. Wu, L. D. Sun, H. P. Zhou and C. H. Yan, *Nanoscale*, 2012, **4**, 3242-3247.

9 O. Metin, S. Ozkar and S. H. Sun, *Nano Res.* 2010, **3**, 676-684.

10 (a) J. Joubert, F. Delbecq, P. Sautet, E. Le Roux, M. Taoufik, C. Thieuleux, F. Blanc, C. Coperet, J. Thivolle-Cazat and J.-M. Basset, *J. Am. Chem. Soc.* 2006, **128**, 9157-9169. (b) R. C. Jin, *Nanotechnol. Rev.* 2012, **1**, 31-56.

11 (a) H. Lim, J. Lee, S. Jin , J. Kim, J. Yoon and T. Hyeon, *Chem. Comm.* 2006, **4**, 463-465. (b) M. Xia, M. Long, Y. Yang, C. Chen, W. Cai and B. Zhou, *Appl. Catal., B* 2011, **110**, 118-125.

12 A. Vinu, K. Z. Hossain and K. Ariga, *J. Nanosci. Nanotechno.* 2005, **5**, 347-371.

13 N. Linares, E. Serrano, M. Rico, A. M. Balu, E. Losada, R. Luque and J. Garcia-Martinez, *Chem. Comm.* 2011, **47**, 9024-9035.

14 D. Margolese, J. A. Melero, S. C. Christiansen, B. F. Chmelka and G. D. Stucky, *Chem. Mater.* 2000, **12**, 2448-2459.

15 A. Sayari and S. Hamoudi, *Chem. Mater.* 2001, **13**, 3151-3168.

16 G. Akiyama, R. Matsuda, H. Sato, M. Takata and S. Kitagawa, *Adv. Mater.* 2011, **23**, 3294–3297.

17 D. Das, J.F. Lee and S. Cheng, *Chem. Commun.* 2001, 2178-2179.

18 D. H. K. Jackson, D. Wang, J. M. R Gallo, A. J. Crisci, S. L .Scott, J. A. Dumesic and T. F. Kuech, *Chem. Mater.* 2013, **25**, 3844-385.

19 H. Kim, S. Prakash, W. E. Mustain and P. A. Kohl, *J. Power Sources*, 2009, **193**, 562-569.

20 S. M. Cohen, *Chem. Rev.* 2012, **112**, 970-1000.

21 S. Che, A. E. Garcia-Bennett, T. Yokoi, K. Sakamoto, H. Kunieda, O. Terasaki and T. Tatsumi. *Nature Mater.* 2003, **2**, 801-805.

22 T. Yokoi, H. Yoshitake and T. Tatsumi, *Chem. Mater.* 2003, **15**, 4536-4538.

23 C. Gao and S. Che, *Adv. Funct. Mater.* 2010, **20**, 2750-2768.

24 T. Yokoi, H. Yoshitake, T. Yamada, Y. Kubota and T. Tatsumi, *J. Mater. Chem.* 2006, **16**, 1125–1135.

25 J. G. Wang, Q. Xiao, H. J. Zhou, P. C. Sun, D. T. Ding, T. H. Chen, *J. Colloid Interf. Sci.* **2008**, *323*, 332-337.

26 H. Zheng, C. Gao and S. Che, *Microporous Mesoporous Mater.* 2008, **116**, 299-307.

27 M. Z. Kassaee and H. Masrouri, F. Movahedi, *Appl. Catal., A* 2011, **395**, 28-33.

28 J. DeLaat and H. E. Gallard, *Environ. Sci. Technol.* 1999, **33**, 2726-2732.

29 (a) G. Zhang, Y. Gao, Y. Zhang and Y. Guo, *Environ. Sci. Technol.* 2010, **44**, 6384–6389. (b) S. Guo, G. Zhang, Y. Guo and J.C. Yu, *Carbon* 2013, **60**, 437-444.

30 V. Umamaheswari, M. Palanichamy and V. Murugesan, *J. Catal.* 2002, **210**, 367-374.

31 S. Hao, Q. Xiao, H. Yang, Y. Zhong, F. Pepe and W. Zhu, *Microporous Mesoporous Mater.* 2010, **132**, 552-558.

32 S. Hao, Y. Zhong, F. Pepe and W. Zhu, *Chem. Eng. J.* 2012, **189-190**, 160-167.

33 W. Wang, X. Zhuang, Q. Zhao and Y. Wan, *J. Mater. Chem.* 2012, **22**, 15874-15886.

34 G. D. Yadav and A. D. Murkute, *Adv. Syn. Catal.* 2004, **346**, 389-394.

35 N. Koukabi, E. Kolvari, M. A. Zolfigol, A. Khazaei, B. S. Shaghasemi and B. Fasahati, *Adv. Syn. Catal.* 2012, **354**, 2001-2008.

36 H. N. Yang, S. H. Cho and W. J. Kim, *J. Membr. Sci.* 2012, **421-422**, 318-326.

37 W. Mao, H. Ma and B. Wang, *J. Hazard. Mater.* 2010, **176**, 361-366.

38 J. Li, J. F. Revol and R. H. Marchessault, *J. Colloid Interf. Sci.* 1997, **192**, 447-457.

39 L. J. Liu, G. L. Zhang, L. Wang, T. Huang and L. Qin, *Ind. Eng. Chem. Res.* 2011, **50**, 7219-7227.

40 L. Qin, X. X. Pan, L. Wang, X. P. Sun, G. L. Zhang and X. W. Guo, *Appl. Catal., B* 2014, **150-151**, 544-553.

41 S. Y. Hao, Q. Xiao, H. Yang, Y. J. Zhong, F. Pepe and W. D. Zhu, *Microporous Mesoporous Mater.* 2010, **132**, 552-558.

42 Y. J. Wu, L. Qin, G.L. Zhang, L. Chen, X. W. Guo and M. Liu, *Ind. Eng. Chem. Res.* 2013, **52**, 16698-16708.

43 L. Qin, G. L. Zhang, Z. Fan, Y. J. Wu, X. W. Guo and M. Liu, *Chem. Eng. J* 2014, **244**, 296-306.

44 L. Guo, F. Chen, X. Fan, W. Cai and J. Zhang, *Appl. Catal., B* 2010, **96**, 162-168.